THE JOURNAL OF PHYSICAL CHEMISTRY C

pubs.acs.org/JPCC Article

Formation of Regular Wormlike Patterns by Dewetting Aqueous Dispersions of Halloysite Nanotubes

Hongzhong Liu, Xiang Cao, Xiaohan Yang, Mingxian Liu,* and Yuri Lvov*

Cite This: J. Phys. Chem. C 2020, 124, 8034−8040 Read Online

ABSTRACT: The wormlike micropatterns were elaborated by drying halloysite clay nanotube dispersions placed between two horizontal glass slides. This 0.1−0.2 mm thick confined space induces the fractal self-assembly of charged nanotubes governed by water evaporation and flow directions. The wriggled stripe clay patterns were formed both on the upper and bottom glass surfaces with width, height, and stripe spacing controlled by halloysite concentrations, space height, drying time, and temperature in the range of 20−80 °C. After separating the slides, the pattern was divided into two identical fractal clay surfaces. Birefringence in the stripes demonstrated the nanotube oriented domains with 50−100 μm length. A model for the pattern formation is proposed relating this phenomenon with the colloidal self-assembly and coffee-ring formation mechanisms. These solid micropatterns can be transferred on polydimethylsiloxane stamps for further polymer imprinting. The technique is simple and scalable and uses water-based natural clay materials, allowing for green chemistry surface processing.

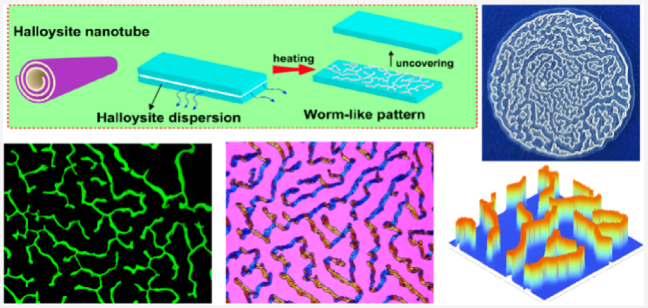

INTRODUCTION

Dewetting is a common phenomenon that can occur at a solid−liquid or liquid−liquid interface. For many applications such as lamination, printing, lubrication, adhesion, and protective coating, dewetting has a crucial importance.[1−4] Recently, it has been found that drying of thin liquid films containing colloids leads to the formation of micro/nanopatterns.[5−8] A "fingering instability" would develop from the rim of initially circular holes, and it becomes more obvious for higher viscosity and entanglements of the polymer molecules.[9] Regular two-dimensional dot arrays and line patterns by dewetting the polystyrene films on a solid substrate were also produced.[10] The liquid−solid−vapor three-phase line is a critical region where pattern formation occurs during drying. Polymer dots, stripes, and ladders were produced ruled by the dewetting, stick−slip motion, and finger instability.[11−13] A spiral pattern of polymethylmethacrylate in toluene can be generated by drying this solution placed between two silicon wafers.[14] A chemical heterogeneous substrate would guide material to specific areas, forming a pattern.[15,16] There are studies focused on the formation of the patterned structures by dewetting the polymer films and nanocrystal dispersions.[17−21] Here, we report the formation of a wriggled stripe pattern by drying an aqueous clay nanotube dispersion sandwiched between two glass slides, with specific features determined by the tubes' orientation.

Halloysite, natural clay nanotube (HNT) mineral, exhibits an empty cylindrical morphology.[22−24] These nanotubes are formed by rolling a 0.72 nm thick kaolin sheet and have a chemical formula $Al_2Si_2O_5(OH)_4{\cdot}nH_2O$, where n = 2 and 0 represent hydrous and anhydrous clay state, respectively. The tube external surface is mainly composed of silanol (Si−OH) groups, whereas the inner lumen surface composition is aluminoxane (Al−OH). The length, inner, and outer diameters are 300−800, 15−20, and 50−70 nm, respectively.[25,26] HNT has a specific surface area of ca. 60 m^2/g and a particle aspect ratio of ca. 10:1. This nanoclay is biocompatible, and it has a high mechanical strength, water-dispersion stability due to high zeta-potential of ca. −30 mV, and thermal stability up to 1300 °C.[27]

The aqueous dispersion self-assembly of these charged clay nanotubes into ordered arrays was recently proposed.[28,29] We reported oriented HNT systems fabricated via mechanisms of "coffee-ring" formation and extended this technique with the production of regular stripe patterns on the inner wall of the capillary. A similar oriented HNT stripe microstructure was formed in the confined space of a vertical slitlike space composed of two glass slides with a sphere-on-flat geometry and brush-assisted deposition.[30,31] Such aligned clay nanotube patterns effectively controlled the oriented growth of mesenchymal stem cells.

Received: February 19, 2020
Revised: March 14, 2020
Published: March 18, 2020

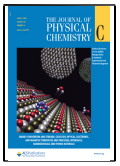

https://dx.doi.org/10.1021/acs.jpcc.0c01424
J. Phys. Chem. C 2020, 124, 8034−8040

In this study, we prepared wormlike nanotube fractal patterns using two parallel glass slides with dewetting of halloysite aqueous dispersions (Scheme 1). The width, height, and area of such solid clay patterns depend on the dispersion concentration, drying temperature, and confined space height. The patterned surface can be used as a template for preparing polydimethylsiloxane (PDMS) stamps for polymer imprinting.

Scheme 1. Experimental Setup and Production of Wormlike Pattern on Glass Slides (a), Images of Halloysite Aqueous Dispersion with Different Concentrations (b), and Formation of Wormlike Pattern from 4 wt % HNT at 60 °C (c)

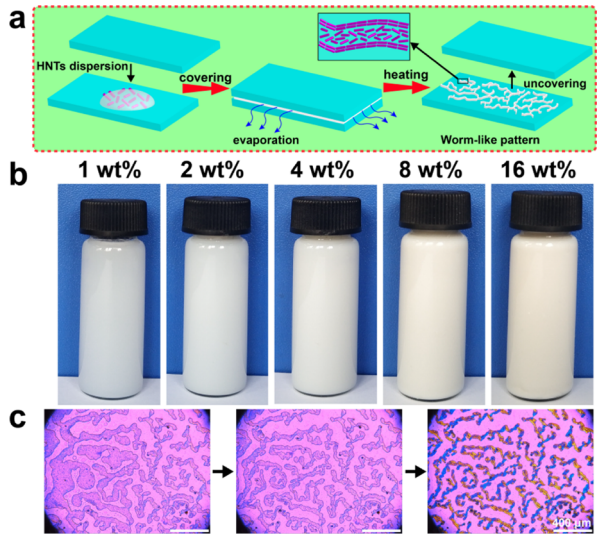

EXPERIMENTAL SECTION

Materials and Characterization. Halloysite was obtained from Guangzhou Runwo Materials Technology Co. Ltd., China. PDMS (analytical-grade) was purchased from Dow Corning Co. Ltd., China. Carboxylated styrene butadiene rubber latex with a solid content of 50 wt % was purchased from Guangzhou Juntai Materials Co. Ltd., China.

We used field emission-scanning electron microscopy (SEM, ULTRA55, Carl Zeiss Jena Co., Germany), transmission electron microscopy (TEM) (JEM-2100F, JEOL Ltd., Japan), and atomic force microscopy (AFM) (Veeco Instrument Inc) for characterization. Fourier transform infrared (FTIR) spectra were obtained with a Thermo FTIR (Nicolet iS50, Thermo Fisher Scientific Co. Ltd., USA) spectrometer. X-ray diffraction (XRD) patterns were recorded using a Miniflex600 diffractometer, Rigaku Corp, Japan, with Cu Kα radiation. The hydrodynamic diameter and surface potential were measured with a zeta potential analyzer (NanoBrook Omni, Brookhaven Instruments Ltd., USA). Nanoclay dewetting was studied with a polarized optical microscope (BX51, Olympus Corp., Japan), a stereo microscope (ZEISS SteREO Discovery V20), and a three-dimensional (3D) profilometer (UP-DUAL MODE, Rtec Engineering Ltd., USA). The surface tension was controlled with a drop-shape analyzer (DSA100, Kruss Ltd., Germany).

Preparation of Dewetting Structures. The preparing process of dewetting clay structures is shown in Scheme 1. HNT dispersion (100 μL) with different concentrations were dropped onto the surface of a glass slide. Another glass slide covered the front glass slide horizontally, and then water was evaporated at the selected temperature between 20 and 80 °C. HNT concentrations were 1, 2, 4, 8, and 16 wt %, volumes were 10, 25, and 50 μL, and heights of the confined space were 80, 160, and 240 μm.

RESULTS AND DISCUSSION

From the SEM and TEM image processing of halloysite, the average tube length and inner and outer diameters are 600 ± 300 and 16 ± 3 and 54 ± 10 nm, respectively. The outer diameters of the tubes were measured as ∼50 nm in the AFM height profile (Figure 1e). FTIR spectrum shows absorption peaks at 3695 and 3623 cm^{-1} which are assigned to the stretching vibration of the inner-surface hydroxyls and the inner hydroxyls (Figure 1).[32] The asymmetric tensile vibration absorption band of Si−O−Si appears around 1018 cm^{-1}, and the O−H deformation of the inner hydroxyl group is at 912 cm^{-1}.[33] The pristine HNT shows Bragg peaks at 2θ = 11.9, 20.0, 24.5, and 35.0° where (001) gives the multilayer wall spacing of 7.4 nm, and (020, 110), (002), and (200,130) are other reflection orders.[34−36] Dynamic light scattering results show the hydrodynamic diameter of 300 ± 10 nm, which corresponds to 3D averaging of single nanotube sizes. The HNT zeta potential was −38 ± 1 mV providing the sample colloidal stability for 10 h.

A halloysite dispersion was sandwiched between two horizontal glass slides and dried at an elevated temperature of 20−80 °C (Scheme 1). At the Scheme 1 bottom, one can see the patterns of wriggling solid clay stripes covering the whole glass area. With the increase of the halloysite concentration, the clay "worms" become thicker and denser. Then, water was evaporated gradually, and the halloysite nanotube assembly was completed within 20 min.

The details of the formation process of the pattern are provided in the Supporting Information and in the video (Figures S1 and Video S1). When water evaporates, the nanotubes move inward because of the meniscus surface tension from shrinking of the liquid film. When the nanotubes were stuck and fixed on the glass, the surface tension of the liquid film reaches equilibrium with the glass friction of the halloysite layer. At this moment, the liquid film stops shrinking in this direction and moves to other directions. This changes the direction of the process, and wormlike patterns are formed. In Video S1, the formation process of the stripe pattern became quicker over time because the contact area of HNT dispersion with air increased during the evaporation process. The alignment of the clay nanotube at a different location of the 15−50 μm width stripe changes as is evident from varying colors in polarized microscopy images (birefringence) (Figure 2). The stripe domains with different colors have preferred orientation of the nanotubes. The clay pattern area and the width of the stripes increased (up to ×5 times) with 1−16 wt % concentration of HNT in dispersion (Figure 2b,c).

Formation of the stripes is the result of competition between surface tension and friction of halloysite tubes with the glass surface. The shrinking distance of the liquid film becomes shorter at higher concentration of HNT dispersion (more numerous nanotubes), which leads to the increase in the stripe width. The viscosity on halloysite dispersion has an influence on the structure of the dewetting pattern (Figure S2).

The dewetting pattern of HNT generates the birefringent effect, and the stripes with different tube orientations show different colors because the first-order retardation plate (λ =

https://dx.doi.org/10.1021/acs.jpcc.0c01424
J. Phys. Chem. C 2020, 124, 8034−8040

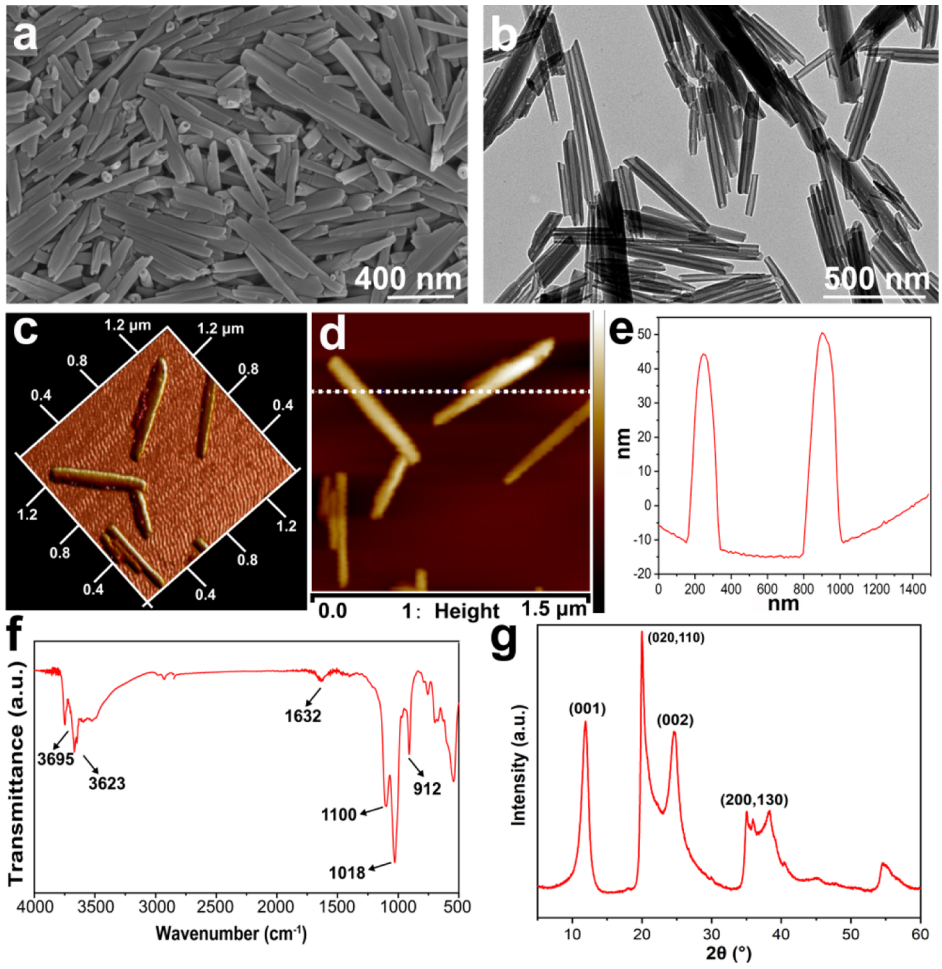

Figure 1. Characterization of halloysite nanotubes: SEM (a), TEM (b), AFM 3D images (c), height (d) and the corresponding profile (e), FTIR (f), and XRD (g).

530 nm) produces an optical path difference. When the orientation angle of the tubes in the stripe is rotated from 0 to 90 or 180 to 270°, the color of the stripe changes from gold to blue (Figure S3). When the orientation angle of the stripe is 45 or 135° between the cross-polarizers, the brightest stripe with blue and gold are observed because most light can pass at 45 or 135°.[37] In other angles, the brightness of stripes reduces during rotation because only a part of light can pass the sample. When the pattern is rotated for 180°, the color of pattern can be recovered. These results suggest an anisotropic structure of the clay nanotube ordering and remind colored polarized images of nematic liquid crystal systems.

The halloysite concentration affects both the width and specific density of the stripes. On our estimations, there are ca. 25, 33, 37, and 43 stripes for 1, 2, 4, and 8 wt %, respectively, and 19 wider stripes for 16 wt % per 2.5 mm (Figure 3). The stereo microscope providing a larger field of view allowed monitoring the formation of the clay patterns. Gold/blue color wormlike stripes are uniformly distributed between the glass with strong contrast to the background, demonstrating a semiordered fractal structure. The stripes are almost uniform in the sample, whereas their width increased with the HNT concentration. Similar wormlike clay patterns were also observed by a fluorescence microscope (Figure S4).

With the increase of the halloysite concentration, wider stripes can be obtained, but their numbers decrease, which is conditioned by HNT mass preservation. The nanotubes in the stripes' boundaries are first stacked to the surface during the drying, fixing aligned nanotubes (Figure S5). However, in the inner region of the stripes, most of the nanotubes are less ordered because they can be freely moved during water evaporation. A few micrometer thickness of the halloysite stripes indicates the multilayer nanotube formations. Figure S5 compares the orientation degree of the nanotubes located inside the stripes and at their vicinity at different distances. Their orientation at the stripe edge is higher than in the middle, which is similar to better orientation of HNT at the edge of "coffee-ring" experiments.[38]

The contact angle of the halloysite dispersion on the glass is one of the factors affecting the shrinking of the liquid film. The higher concentrations of dispersion exhibit bigger contact angle (Figure S6). The contact angle of dispersion is affected by nanotubes' concentration because the nanotubes tend to bundle together in liquid at high concentrations. The hydrogen-bonding interactions among the tubes are more effective as the distance of the tubes decreases. In the same volume of dispersion, the distance between single nanotubes becomes smaller as the concentration increases. As a result, the liquid droplet prefers to shrink to maintain a high contact angle.[39] The contact angle further leads to different surface tensions and heights of HNT arrays in the confined space. The contact angle increases with concentration approaching 16 wt

https://dx.doi.org/10.1021/acs.jpcc.0c01424
J. Phys. Chem. C 2020, 124, 8034−8040

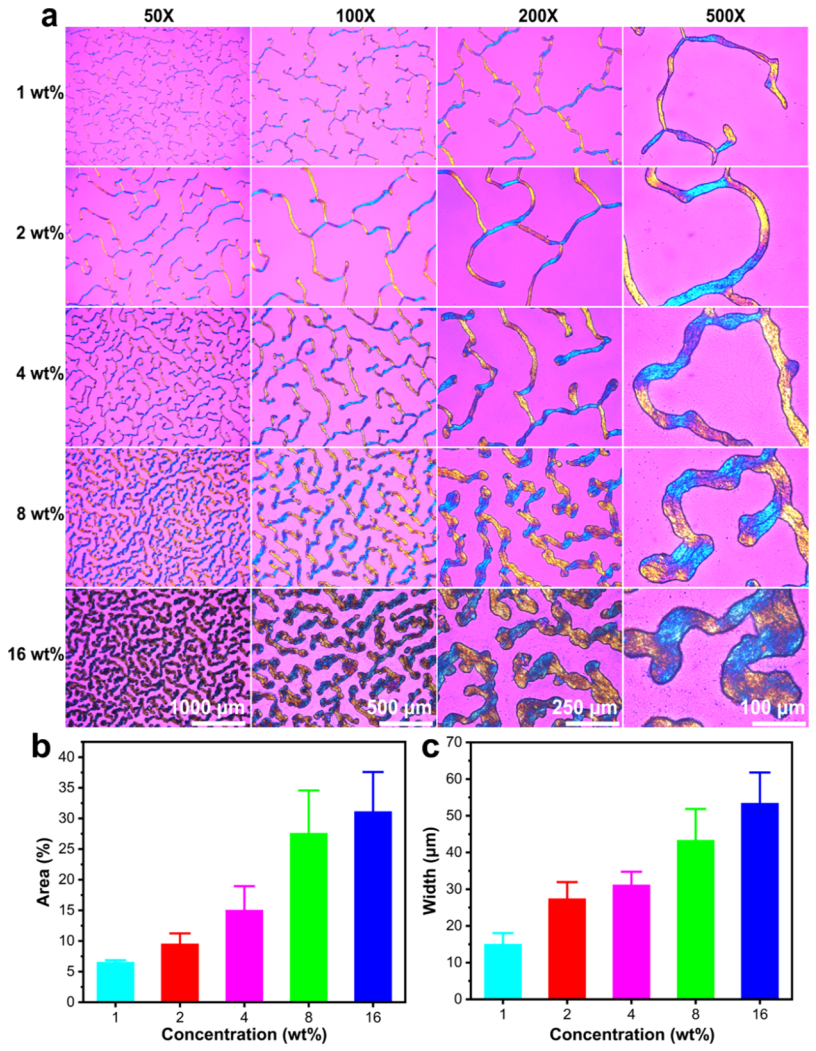

Figure 2. Polarized light microscopy images of HNT "worms" between two slides: dewetting pattern formed at different concentrations of HNT (a), area percentage (b), and width of the stripes (c).

% with proportional increase of the stripe height from 7 to 46 μm (Figure S6). At higher concentrations, the halloysite stripes tend to shrink because of larger surface tension, and their heights for 1, 2, 4, 8, and 16 wt % HNT dispersion are 6.9 ± 0.1, 14.7 ± 0.2, 19.3 ± 0.2, 25.6 ± 0.4, and 46.2 ± 0.7 μm, respectively. The height of the dewetting pattern in the separated bottom slide was characterized by a 3D optical profilometer (Figure 4). The height of the dewetting bottom pattern for 1, 2, 4, 8, and 16 wt % HNT dispersion is 2.8 ± 0.1, 6.2 ± 0.2, 7.5 ± 0.1, 10.6 ± 0.2, and 22.7 ± 0.9 μm, respectively, and it is close to half of the height of the initial not separated patterns.

The evaporation temperature can affect the formation of the wormlike pattern because water in the halloysite dispersion will freeze at 0 °C and boil at 100 °C, which would prevent the pattern formation. Therefore, 20 °C is suitable to be a start evaporation temperature because it is close to room temperature. The temperature of 80 °C is 60 °C higher than 20 °C, which is enough to reflect the effect of temperature on the pattern formation process. As the drying temperature increases from 20 to 80 °C, the stripe width also gradually increases (Figure S7). For 4 wt. % HNT dispersion, it increased from 9 ± 1 to 42 ± 7 μm. The higher evaporation temperature reduces surface tension of the dispersion, thus diminishing the compression force on the wet stripes and widening them.

The effect of confined height and dispersion volume on the clay pattern: the volume of the HNT dispersion was fixed as 25 μL; the concentration was 16 wt %; and the formed clay patterns were pressed between two glass slides (Figure S8). The circle area of the dewetting pattern decreased as the confined space height increased, and the number of nanotubes in a single stripe contained in 80 μm height space is less than that in 160 and 240 μm heights. Capillary force is defined by liquid/solid adhesion and the surface tension due to cohesion. The value of Laplace pressure (P_L) caused by the meniscus is as follows[40]

$$\Delta P_L = 2\sigma/R \quad (1)$$

where σ is the liquid surface tension and R is the radius of the meniscus; σ is proportional to the halloysite concentration, and $2R$ is approximately equal to the distance between two slides (the pattern height). At the constant σ (the same concentration of dispersion), the pressure decreased as the height increased. When the confined space height is minimal of 80 μm, the capillary force is maximized. The large capillary force was balanced by higher friction of halloysite with glass, compressing the stripe width and increasing the HNT

https://dx.doi.org/10.1021/acs.jpcc.0c01424
J. Phys. Chem. C 2020, 124, 8034−8040

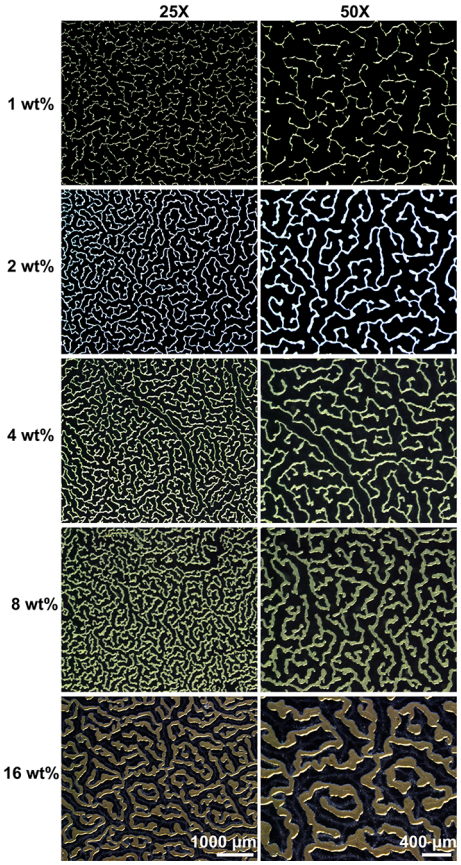

Figure 3. Stereo microscope images of the clay dewetting patterns between two slides produced at different halloysite concentrations.

concentration, minimizing the stripe width. When the height of the confined space increased causing the capillary force to reduce, the stripes become wider of ca. 370 μm. This allows for tailoring the patterns by variation of the confined spacing height.

The area of dewetting clay patterns increased with the dispersion volume (Figure S9). Because the height of the confined space and the dispersion concentration were the same, the capillary force between the liquid film and the glass slide was also the same according to 1. The same capillary force compressed the dispersion droplet to similar diameter, with the formation of identical width stripes. Prepared solid clay fractal structures can be used as molds to reproduce microreliefs on the polymeric surface.

The aspect ratio and hydrophilicity of substrates also affect the formation of the wormlike pattern. The major-axis/minor-axis aspect of the used HNTs is about 8.6 (calculated from TEM images). According to the previous research, spherical particles (major-axis/minor-axis aspect $\alpha = 1$) tended to form a "coffee-ring" pattern, and the HNTs with a very high axis ratio (α = 13.2) could effectively produce a relatively uniform orientation pattern.[38,41,42] Therefore, the suitable aspect ratio of 8.6 with a special confined space, which changes the evaporation direction, could form the wormlike pattern. The hydrophilicity of substrates is another factor which influences the pattern formation. Glass and polypropylene (PP) are used to compare the effect of different substrates. It was found that the wormlike pattern could not form on PP surfaces because the HNT dispersion was very ready to be dewetted between the confined space during evaporation owing to the high

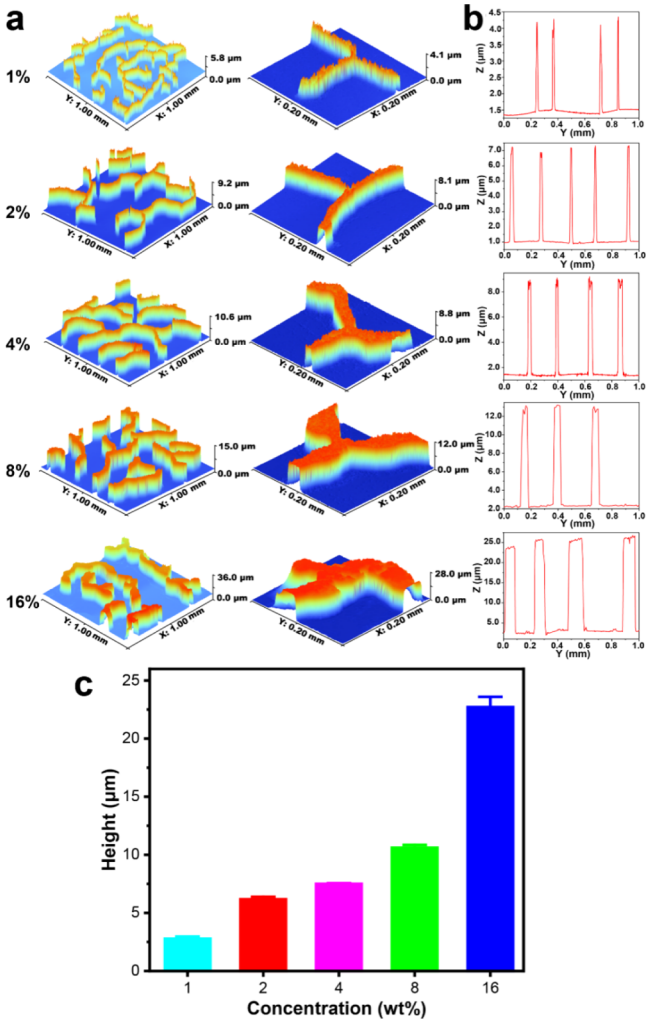

Figure 4. 3D topographic images, roughness curve, and overaged height of the dewetting bottom pattern at different HNT concentrations (a–c).

contact angle. The nanotubes cannot adhere to the surfaces well, and the friction of halloysite dispersion with a PP substrate cannot reach a balance with the capillary forces. As a result, randomly distributed tubes on the PP substrate surface were formed.

PDMS mold was used to imprint in carboxylated styrene-butadiene rubber, and microchannels in the rubber corresponded to the width and height of the clay stripes. Therefore, the halloysite patterns can be replicated by a simple PDMS template and further imprinted in a latex making controllable fractal surface, for example, for enhanced hydrophobicity. The described clay pattern formation also explains the recently discovered halloysite assembly in the gaps between cuticles on the hair surface .[43]

CONCLUSIONS

Dewetting process of the thin liquid film containing nanotubes confined between two parallel glass slides allowed for fabrication of wormlike fractal micropatterns. The formation of clay nanotube patterns was optimized, and an explanation of the wriggling stripe formation was suggested. Birefringence phenomenon in the clay stripes indicates aligned nanotube domains of 100–200 μm along the "worm" patterns, with

https://dx.doi.org/10.1021/acs.jpcc.0c01424
J. Phys. Chem. C 2020, 124, 8034–8040

better orientation at the edges. The width of the wormlike stripe pattern increases with the dispersion concentration, drying temperature, and distance between the slides, and the stripe height may be adjusted too. Such a fractal surface with controlled clay stripe sizes can be used for preparation of PDMS molding to fabricate patterned plastic surfaces via soft matter imprinting.

■ ASSOCIATED CONTENT

Supporting Information

The Supporting Information is available free of charge at https://pubs.acs.org/doi/10.1021/acs.jpcc.0c01424.

Schematic illustration of the formation of a wormlike pattern and the related self-assembly process of halloysite; photograph, micrograph of edge, micrograph of middle of dewetting pattern of HNT@PVA in glass; polarized optical microscopy images; dewetting pattern rotated at different angles; fluorescence micrographs of the dewetting pattern which was marked by fluorescein isothiocyanate; SEM images of the dewetting pattern formed from different halloysite dispersions, comparison of the orientation state of the nanotubes around the stripes, orientation distributions of the nanotubes far and close to the stripes; contact angle images and result of different concentrations of HNT aqueous dispersions, height of confined space formed at different concentrations of dispersions; polarized light microscopy images and stripe width of the HNT dewetting pattern formed at different drying temperatures; photograph, area ratio, and stripe width of the halloysite dewetting pattern formed at different heights of confined space by using 16 wt % HNT dispersion; and photograph, area ratio, and stripe width of the halloysite dewetting pattern formed at different volumes by using 16 wt % (PDF)

Formation process of the stripe pattern (MP4)

■ AUTHOR INFORMATION

Corresponding Authors

Mingxian Liu − *Department of Materials Science and Engineering, Jinan University, Guangzhou 510632, China; Institute for Micromanufacturing, Louisiana Tech University, Ruston, Louisiana 71272, United States;* orcid.org/0000-0002-5466-3024; Email: liumx@jnu.edu.cn

Yuri Lvov − *Institute for Micromanufacturing, Louisiana Tech University, Ruston, Louisiana 71272, United States;* orcid.org/0000-0003-0722-5643; Email: ylvov@latech.edu

Authors

Hongzhong Liu − *Department of Materials Science and Engineering, Jinan University, Guangzhou 510632, China*

Xiang Cao − *Department of Materials Science and Engineering, Jinan University, Guangzhou 510632, China*

Xiaohan Yang − *Department of Materials Science and Engineering, Jinan University, Guangzhou 510632, China*

Complete contact information is available at: https://pubs.acs.org/10.1021/acs.jpcc.0c01424

Notes

The authors declare no competing financial interest.

■ ACKNOWLEDGMENTS

This work was financially supported by the National Natural Science Foundation of China (51502113), the Guangdong Basic and Applied Basic Research Foundation (2019A1515011509), and the Fundamental Research Funds for the Central Universities (21619102).

■ REFERENCES

(1) Wang, X. D.; Lee, D. J.; Peng, X. F.; Lai, J. Y. Spreading Dynamics and Dynamic Contact Angle of Non-Newtonian Fluids. *Langmuir* **2007**, *23*, 8042−8047.

(2) Wang, X. D.; Zhang, Y.; Lee, D. J.; Peng, X. F. Spreading of Completely Wetting or Partially Wetting Power-Law Fluid on Solid Surface. *Langmuir* **2007**, *23*, 9258−9262.

(3) Craster, R. V.; Matar, O. K. Dynamics and Stability of Thin Liquid Films. *Rev. Mod. Phys.* **2009**, *81*, 1131−1198.

(4) Lu, G.; Wang, X.-D.; Duan, Y.-Y. A Critical Review of Dynamic Wetting by Complex Fluids: From Newtonian Fluids to Non-Newtonian Fluids and Nanofluids. *Adv. Colloid Interface Sci.* **2016**, *236*, 43−62.

(5) Reiter, G. Dewetting of Thin Polymer Films. *Phys. Rev. Lett.* **1992**, *68*, 75−78.

(6) Sharma, A.; Jameel, A. T. Nonlinear Stability, Rupture, and Morphological Phase Separation of Thin Fluid Films on Apolar and Polar Substrates. *J. Colloid Interface Sci.* **1993**, *161*, 190−208.

(7) Stange, T. G.; Evans, D. F.; Hendrickson, W. A. Nucleation and Growth of Defects Leading to Dewetting of Thin Polymer Films. *Langmuir* **1997**, *13*, 4459−4465.

(8) Lee, L.-T.; da Silva, M. d. C. V.; Galembeck, F. Dewetting Patterns of Thin Films of Charged Polymer Solutions. *Langmuir* **2003**, *19*, 6717−6722.

(9) Reiter, G. Unstable Thin Polymer Films: Rupture and Dewetting Processes. *Langmuir* **1993**, *9*, 1344−1351.

(10) Karthaus, O.; Gråsjö, L.; Maruyama, N.; Shimomura, M. Formation of Ordered Mesoscopic Polymer Arrays by Dewetting. *Int. J. Bifurcat. Chaos* **1999**, *9*, 308−314.

(11) Yabu, H.; Shimomura, M. Preparation of Self-Organized Mesoscale Polymer Patterns on a Solid Substrate: Continuous Pattern Formation from a Receding Meniscus. *Adv. Funct. Mater.* **2005**, *15*, 575−581.

(12) Becerril, H. A.; Roberts, M. E.; Liu, Z.; Locklin, J.; Bao, Z. High-Performance Organic Thin-Film Transistors through Solution-Sheared Deposition of Small-Molecule Organic Semiconductors. *Adv. Mater.* **2008**, *20*, 2588−2594.

(13) Liu, N.; Zhou, Y.; Wang, L.; Peng, J.; Wang, J.; Pei, J.; Cao, Y. In Situ Growing and Patterning of Aligned Organic Nanowire Arrays via Dip Coating. *Langmuir* **2009**, *25*, 665−671.

(14) Peng, J.; Wang, H.; Li, B.; Han, Y. Pattern Formation in a Confined Polymer Film induced by a Temperature Gradient. *Polymer* **2004**, *45*, 8013−8017.

(15) Lopez, G.; Biebuyck, H.; Frisbie, C.; Whitesides, G. Imaging of Features on Surfaces by Condensation Figures. *Science* **1993**, *260*, 647−649.

(16) Biebuyck, H. A.; Whitesides, G. M. Self-Organization of Organic Liquids on Patterned Self-Assembled Monolayers of Alkanethiolates on Gold. *Langmuir* **1994**, *10*, 2790−2793.

(17) Sharma, A.; Khanna, R. Pattern Formation in Unstable Thin Liquid Films. *Phys. Rev. Lett.* **1998**, *81*, 3463−3466.

(18) Reiter, G.; Sharma, A.; Casoli, A.; David, M.-O.; Khanna, R.; Auroy, P. Thin Film Instability Induced by Long-Range Forces. *Langmuir* **1999**, *15*, 2551−2558.

(19) Schwartz, L. W.; Roy, R. V.; Eley, R. R.; Petrash, S. Dewetting Patterns in a Drying Liquid Film. *J. Colloid Interface Sci.* **2001**, *234*, 363−374.

(20) Lu, G.; Li, W.; Yao, J.; Zhang, G.; Yang, B.; Shen, J. Fabricating Ordered Two-Dimensional Arrays of Polymer Rings with Submicrometer-Sized Features on Patterned Self-Assembled Monolayers by Dewetting. *Adv. Mater.* **2002**, *14*, 1049−1053.

(21) Luo, C.; Xing, R.; Han, Y. Ordered Pattern Formation from Dewetting of Polymer Thin Film with Surface Disturbance by Capillary Force Lithography. *Surf. Sci.* **2004**, *552*, 139−148.
(22) Lvov, Y.; Abdullayev, E. Functional Polymer−Clay Nanotube Composites with Sustained Release of Chemical Agents. *Prog. Polym. Sci.* **2013**, *38*, 1690−1719.
(23) Liu, M.; Jia, Z.; Jia, D.; Zhou, C. Recent Advance in Research on Halloysite Nanotubes-Polymer Nanocomposite. *Prog. Polym. Sci.* **2014**, *39*, 1498−1525.
(24) Huang, B.; Liu, M.; Long, Z.; Shen, Y.; Zhou, C. Effects of Halloysite Nanotubes on Physical Properties and Cytocompatibility of Alginate Composite Hydrogels. *Mater. Sci. Eng. Carbon* **2017**, *70*, 303−310.
(25) Joussein, E.; Petit, S.; Churchman, J.; Theng, B.; Righi, D.; Delvaux, B. Halloysite Clay Minerals − a review. *Clay Miner.* **2005**, *40*, 383−426.
(26) Ye, Y.; Chen, H.; Wu, J.; Chan, C. M. Interlaminar Properties of Carbon Fiber Composites with Halloysite Nanotube-Toughened Epoxy Matrix. *Compos. Sci. Technol.* **2011**, *71*, 717−723.
(27) Lvov, Y.; Wang, W.; Zhang, L.; Fakhrullin, R. Halloysite Clay Nanotubes for Loading and Sustained Release of Functional Compounds. *Adv. Mater.* **2016**, *28*, 1227−1250.
(28) Byun, M.; Bowden, N. B.; Lin, Z. Hierarchically Organized Structures Engineered from Controlled Evaporative Self-Assembly. *Nano Lett.* **2010**, *10*, 3111−3117.
(29) Byun, M.; Han, W.; Qiu, F.; Bowden, N. B.; Lin, Z. Hierarchically Ordered Structures Enabled by Controlled Evaporative Self-Assembly. *Small* **2010**, *6*, 2250−2255.
(30) He, R.; Liu, M.; Shen, Y.; Long, Z.; Zhou, C. Large-Area Assembly of Halloysite Nanotubes for Enhancing the Capture of Tumor Cells. *J. Mater. Chem. B* **2017**, *5*, 1712−1723.
(31) Liu, M.; Huo, Z.; Liu, T.; Shen, Y.; He, R.; Zhou, C. Self-Assembling Halloysite Nanotubes into Concentric Ring Patterns in a Sphere-on-Flat Geometry. *Langmuir* **2017**, *33*, 3088−3098.
(32) Ledoux, R. L.; White, J. L. Infrared Study of the OH Groups in Expanded Kaolinite. *Science* **1964**, *143*, 244−246.
(33) Szczepanik, B.; Słomkiewicz, P.; Garnuszek, M.; Czech, K.; Banaś, D.; Kubala-Kukuś, A.; Stabrawa, I. The Effect of Chemical Modification on the Physico-Chemical Characteristics of Halloysite: FTIR, XRF, and XRD Studies. *J. Mol. Struct.* **2015**, *1084*, 16−22.
(34) Brindley, G. W.; Robinson, K.; Macewan, D. M. C. The Clay Minerals Halloysite and Meta-Halloysite. *Nature* **1946**, *157*, 225−226.
(35) Deng, S.; Zhang, J.; Ye, L.; Wu, J. Toughening Epoxies with Halloysite Nanotubes. *Polymer* **2008**, *49*, 5119−5127.
(36) Lvov, Y. M.; Shchukin, D. G.; Möhwald, H.; Price, R. R. Halloysite Clay Nanotubes for Controlled Release of Protective Agents. *ACS Nano* **2008**, *2*, 814−820.
(37) Wu, S.-T.; Efron, U.; Hess, L. D. Birefringence Measurements of Liquid Crystals. *Appl. Opt.* **1984**, *23*, 3911−3915.
(38) Zhao, Y.; Cavallaro, G.; Lvov, Y. Orientation of Charged Clay Nanotubes in Evaporating Droplet Meniscus. *J. Colloid Interface Sci.* **2015**, *440*, 68−77.
(39) Vafaei, S.; Borca-Tasciuc, T.; Podowski, M. Z.; Purkayastha, A.; Ramanath, G.; Ajayan, P. M. Effect of Nanoparticles on Sessile Droplet Contact Angle. *Nanotechnology* **2006**, *17*, 2523−2527.
(40) Butt, H.-J.; Kappl, M. Normal Capillary Forces. *Adv. Colloid Interface Sci.* **2009**, *146*, 48−60.
(41) Yunker, P. J.; Still, T.; Lohr, M. A.; Yodh, A. G. Suppression of the Coffee-Ring Effect by Shape-Dependent Capillary Interactions. *Nature* **2011**, *476*, 308−311.
(42) Qin, L.; Zhao, Y.; Liu, J.; Hou, J.; Zhang, Y.; Wang, J.; Zhu, J.; Zhang, B.; Lvov, Y.; Van der Bruggen, B. Oriented Clay Nanotube Membrane Assembled on Microporous Polymeric Substrates. *ACS Appl. Mater. Interfaces* **2016**, *8*, 34914−34923.
(43) Panchal, A.; Fakhrullina, G.; Fakhrullin, R.; Lvov, Y. Self-assembly of Clay Nanotubes on Hair Surface for Medical and Cosmetic Formulations. *Nanoscale* **2018**, *10*, 18205−18216.

https://dx.doi.org/10.1021/acs.jpcc.0c01424
J. Phys. Chem. C 2020, 124, 8034−8040

Supporting Information

Formation of Regular Worm-like Patterns by Dewetting Aqueous Dispersions of Halloysite Nanotubes

Hongzhong Liu[1], Xiang Cao[1], Xiaohan Yang[1], Mingxian Liu[1,2], Yuri Lvov[2] **

[1]Department of Materials Science and Engineering, Jinan University, Guangzhou 510632, China

[2]Institute for Micromanufacturing, Louisiana Tech University, Ruston, LA 71272, USA

*To whom all correspondence should be addressed.

Email: liumx@jnu.edu.cn;

Email: ylvov@latech.edu.

Number of Pages: 6

Number of Figures: 9

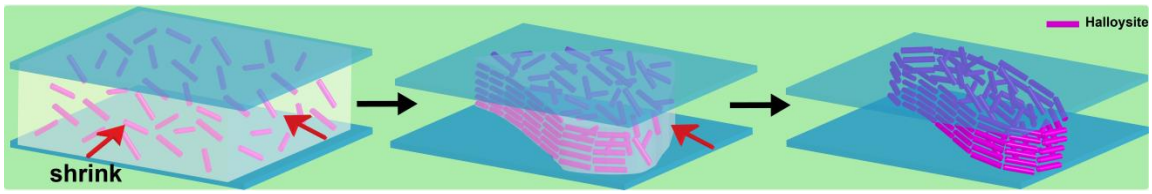

Figure S1. Schematic illustration of the formation of worm-like pattern and the related self-assembly process of halloysite.

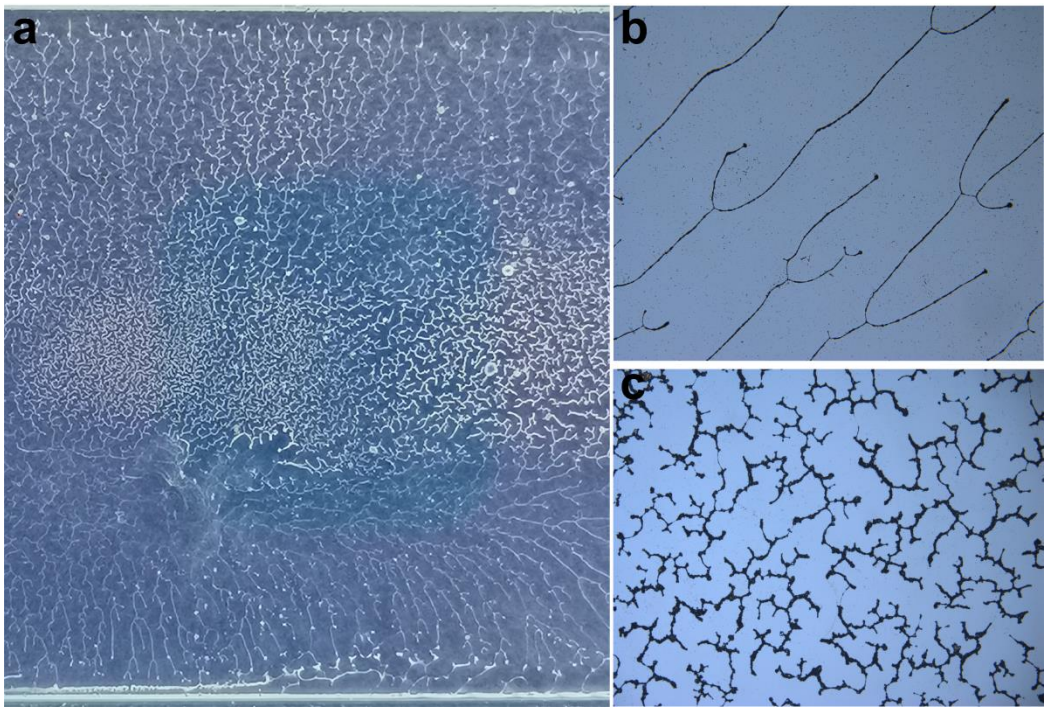

Figure S2. Photograph (a), Micrograph of edge (b), Micrograph of middle of dewetting pattern of HNT@PVA in glass (c).

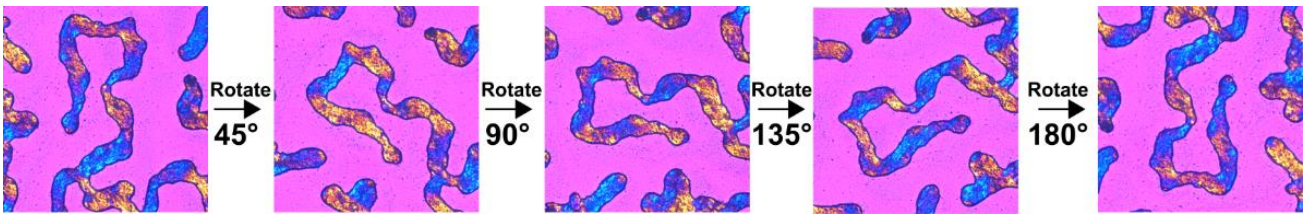

Figure S3. The POM images: the dewetting pattern rotated at different angle.

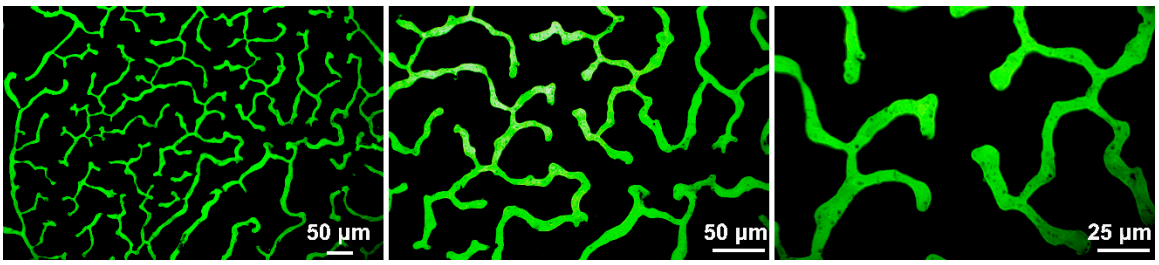

Figure S4. Fluorescence micrographs of dewetting pattern which was marked by FITC.

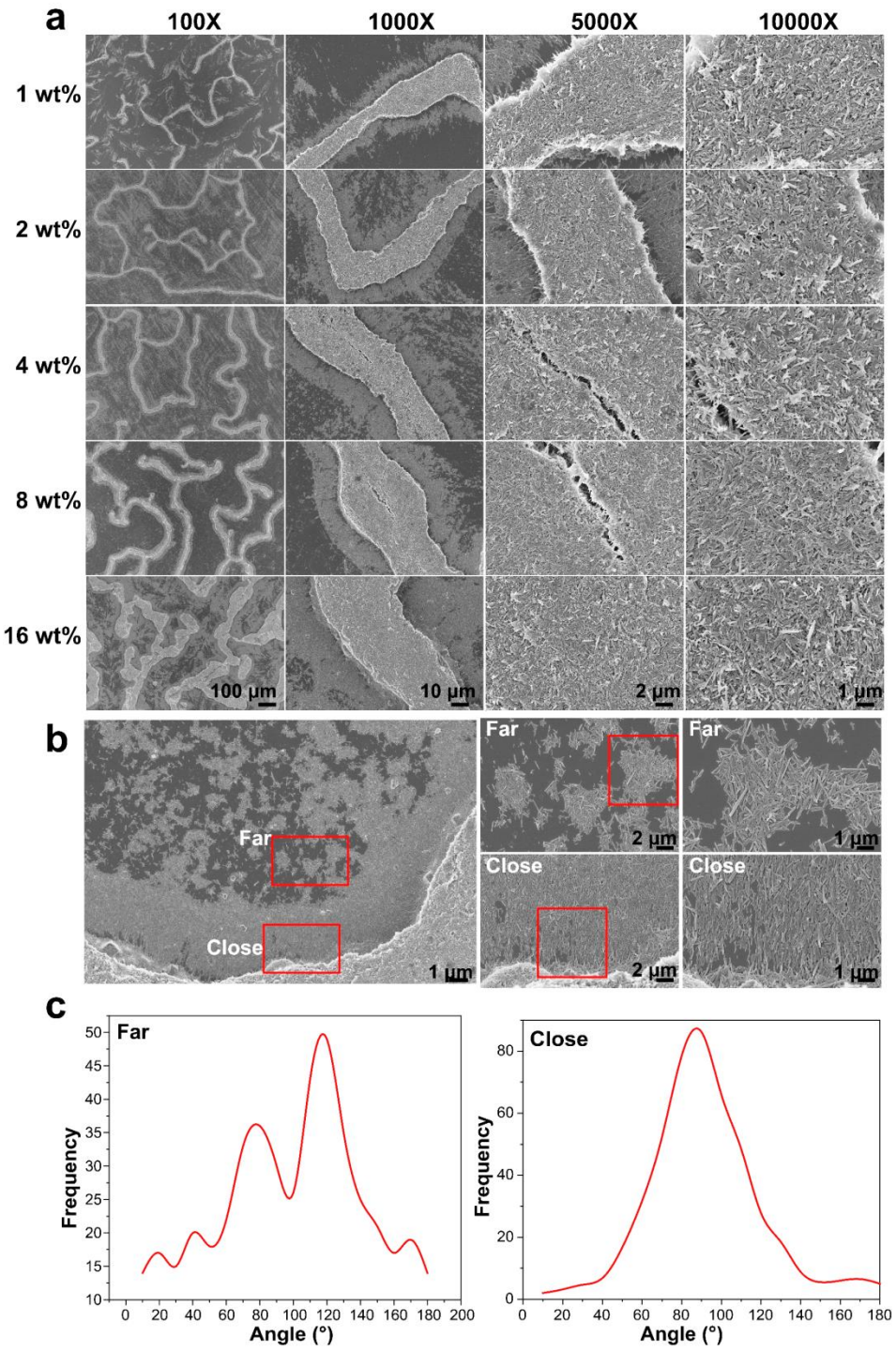

Figure S5. SEM images of the detwetting pattern formed from different halloysite dispersion (a), The comparison of the orientation state of the nanotubes around the stripes (b) , The orientation distributions of the nanotubes far and close to the stripes (c).

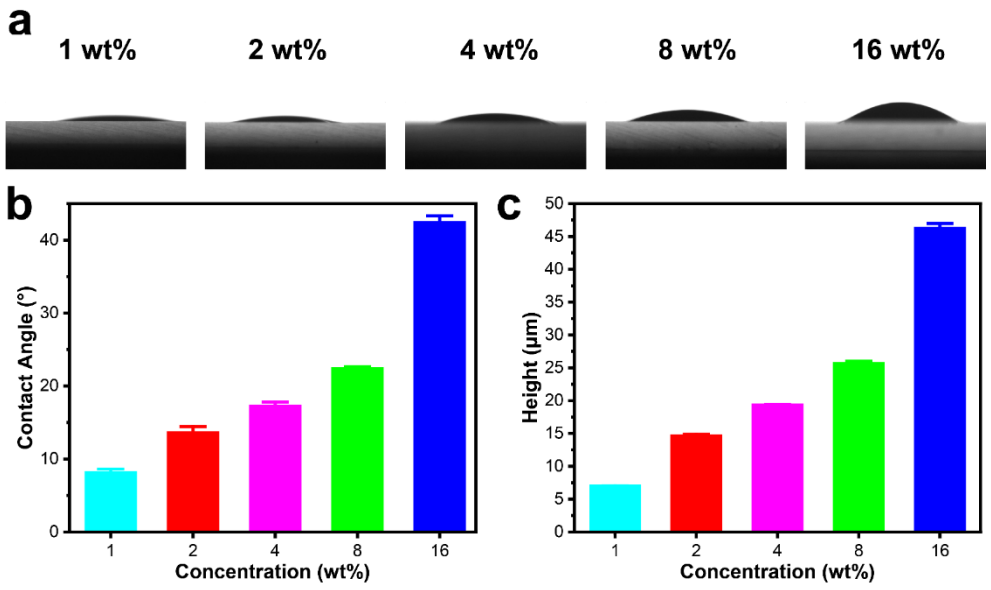

Figure S6. Contact angle images (a) and result of different concentrations of HNT aqueous dispersion (b), Height of confined space formed at the different concentrations of dispersion (c).

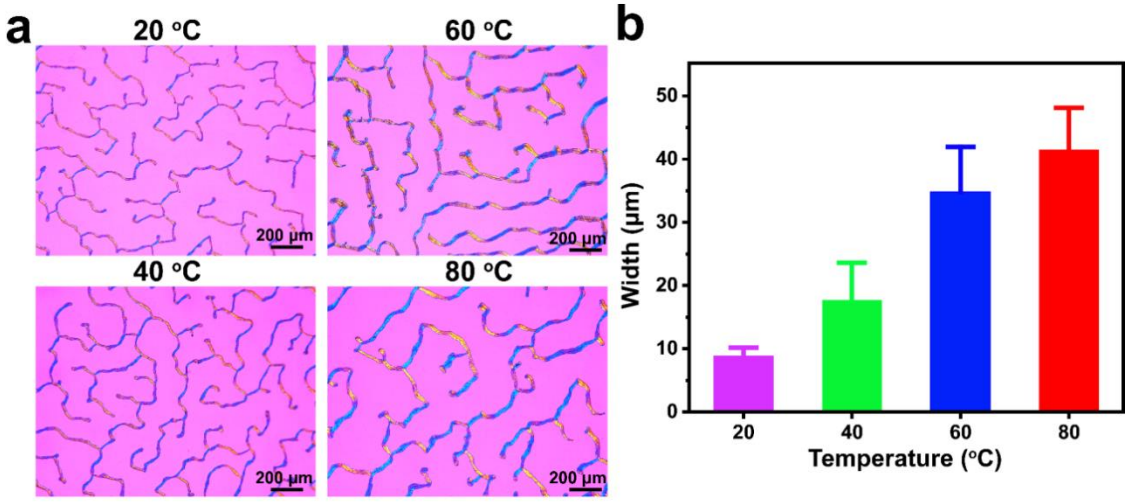

Figure S7. Polarized light microscopy images (a) and stripe width of HNT dewetting pattern formed at the different drying temperatures (b).

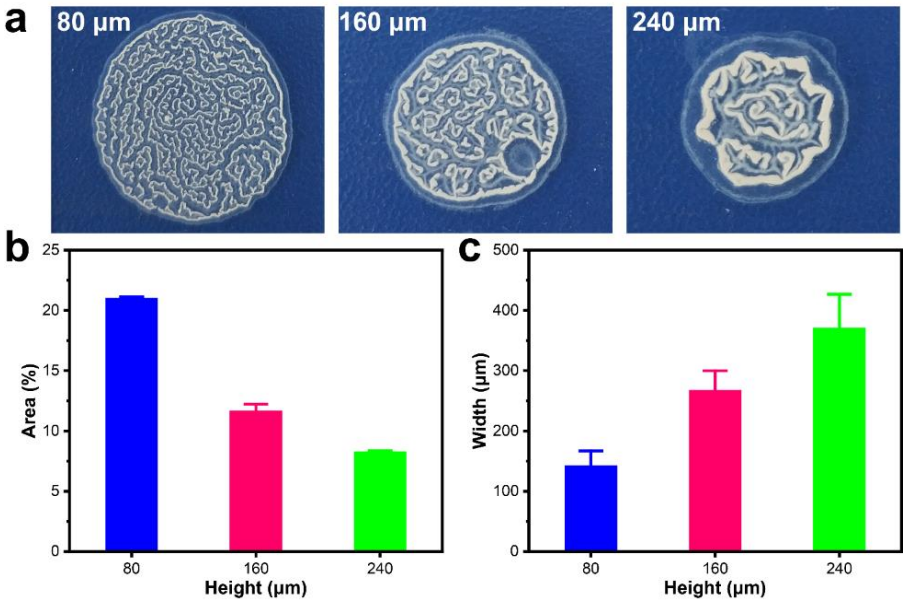

Figure S8. Photograph (a), area ratio (b), and stripe width (c) of halloysite dewetting pattern formed at the different height of confined space by using 16 wt.% HNTs dispersion.

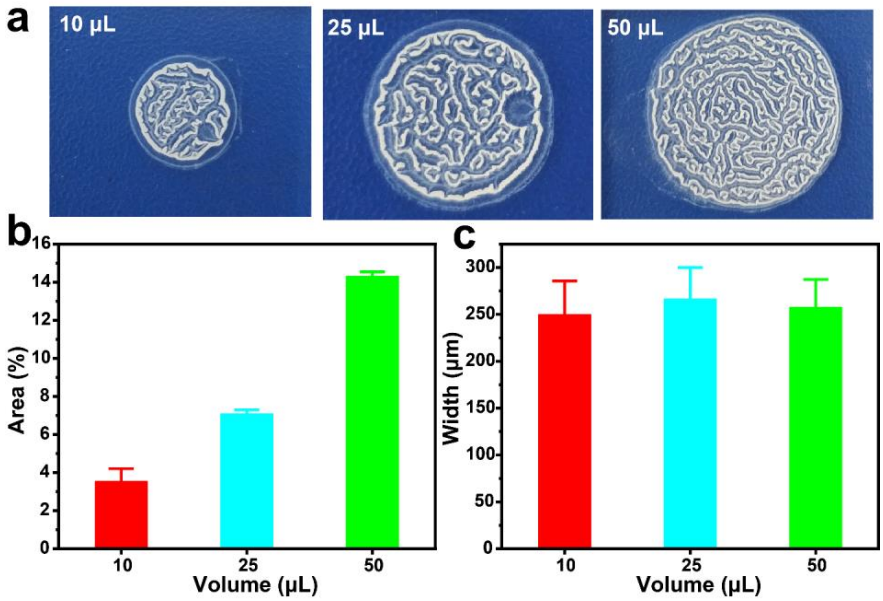

Figure S9. Photograph (a), area ratio (b), and stripe width (c) of halloysite dewetting pattern formed at the different volume by using 16 wt.% HNT dispersion.